NASA-CR-201044

Applied Optics

20 SEPTEMBER 1994

LASERS, PHOTONICS, AND ENVIRONMENTAL OPTICS

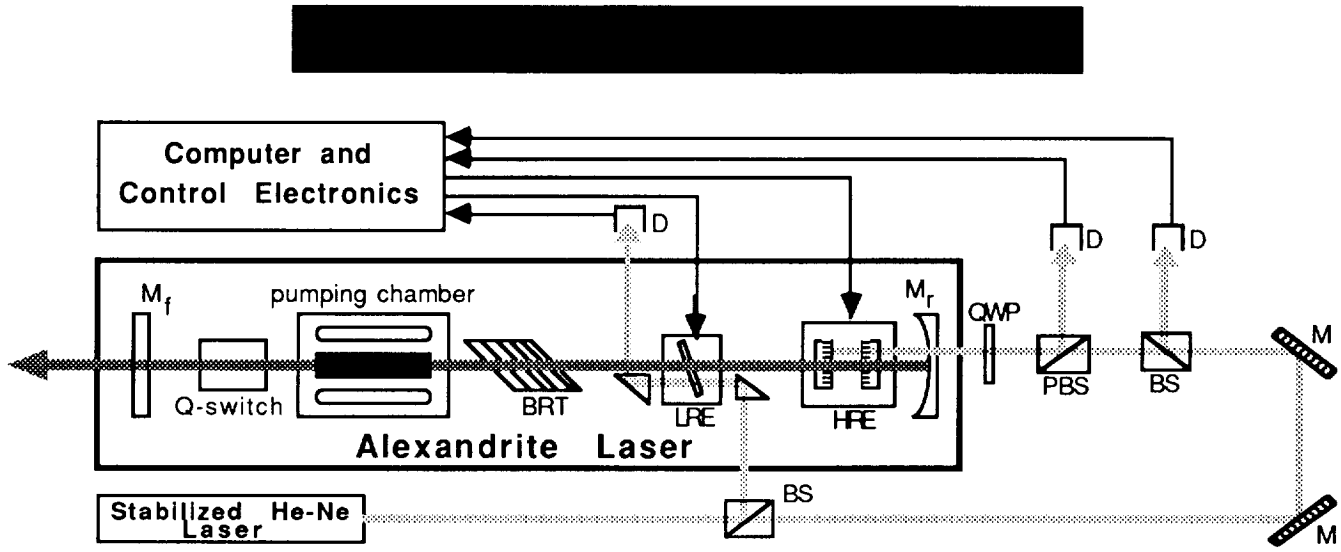

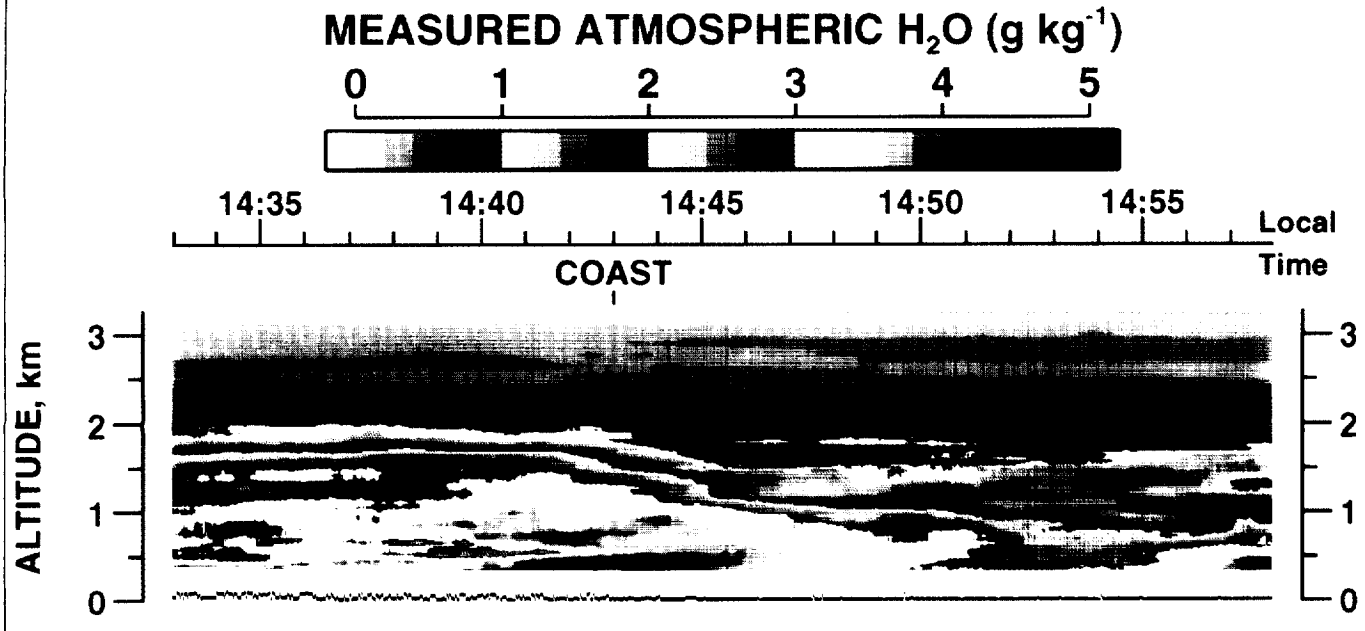

Airborne differential absorption lidar system for measurements of atmospheric water vapor and aerosols

Noah S. Higdon, Edward V. Browell, Patrick Ponsardin, Benoist E. Grossmann, Carolyn F. Butler, Thomas H. Chyba, M. Neale Mayo, Robert J. Allen, Alene W. Heuser, William B. Grant, Syed Ismail, Shane D. Mayor, and Arlen F. Carter

An airborne differential absorption lidar (DIAL) system has been developed at the NASA Langley Research Center for remote measurements of atmospheric water vapor (H_2O) and aerosols. A solid-state alexandrite laser with a 1-pm linewidth and >99.85% spectral purity was used as the on-line transmitter. Solid-state avalanche photodiode detector technology has replaced photomultiplier tubes in the receiver system, providing an average increase by a factor of 1.5–2.5 in the signal-to-noise ratio of the H_2O measurement. By incorporating advanced diagnostic and data-acquisition instrumentation into other subsystems, we achieved additional improvements in system operational reliability and measurement accuracy. Laboratory spectroscopic measurements of H_2O absorption-line parameters were performed to reduce the uncertainties in our knowledge of the absorption cross sections. Line-center H_2O absorption cross sections were determined, with errors of 3–6%, for more than 120 lines in the 720-nm region. Flight tests of the system were conducted during 1989–1991 on the NASA Wallops Flight Facility Electra aircraft, and extensive intercomparison measurements were performed with dew-point hygrometers and H_2O radiosondes. The H_2O distributions measured with the DIAL system differed by $\leq 10\%$ from the profiles determined with the *in situ* probes in a variety of atmospheric conditions.

Key words: Differential absorption lidar, alexandrite laser, water vapor, aerosols.

Introduction

Water vapor (H_2O) is the most variable of the major molecular constituents of the atmosphere, and it plays a primary role in many aspects of atmospheric physics, including processes involved in meteorology, climate, the Earth's radiation budget, and the global hydrological cycle. In addition, H_2O can be used as a tracer in studies of atmospheric transport and chemistry. Therefore measurements of the spatial and temporal distribution of H_2O will lead to a better understanding of the various dynamic and chemical processes that occur in the atmosphere. An airborne differential absorption lidar (DIAL) can make the necessary high-resolution measurements of H_2O and aerosols over large regions of the lower atmosphere. This paper describes the design, development, and application of an airborne H_2O DIAL system for the remote detection of H_2O and aerosol profiles in the atmosphere.

Several researchers have developed and implemented ground-based lidar systems to determine the vertical concentration profiles of H_2O remotely.[1–5] These facilities include both Raman lidar, which incorporates inelastic backscattering to generate a return signal that is shifted in frequency from the frequency of the transmitted signal, and DIAL, in which elastic backscattering is combined with absorption to produce a range-resolved profile. The capabili-

N. S. Higdon, E. V. Browell, W. B. Grant, S. Ismail, and A. F. Carter are with the Atmospheric Sciences Division, NASA Langley Research Center, MS 401A, Hampton, Virginia 23681-0001; P. Ponsardin, C. F. Butler, and S. D. Mayor are with the Science and Applications International Corporation, 1 Enterprise Parkway, Suite 250, Hampton, Virginia 23666. When this work was performed, B. E. Grossmann and A. W. Heuser were with STX Corporation, 17 Research Drive, Hampton, Virginia 23665; B. E. Grossmann is now with Thomson-CSF, Rue Guynemer, BP55, 78283 Guyancourt, Cedex, France; A. W. Heuser is now with Harris Corporation, GCSD, M/S 1-52842, P.O. Box 91000, Melbourne, Florida 32902. T. H. Chyba is with the National Research Council, MS 401A, Hampton, Virginia 23681-0001; N. M. Mayo is with Lockheed Engineering and Sciences Company, 144 Research Drive, Hampton, Virginia 23666; and R. J. Allen is with Allen Associates, 48 Diamond Hill Road, Hampton, Virginia 23666.

Received 5 February 1993; revised manuscript received 17 November 1993.

0003-6935/94/276422-17$06.00/0.

a reprint from Applied Optics

ties of many ground-based lidar systems have been enhanced by having them mounted on mobile platforms for measurements in diverse climates and under various atmospheric conditions.[6-8] To increase the flexibility of the lidar measurements further and to provide for mesoscale observations, one can design lidar systems to operate on airborne platforms. Because of the low-level return signals and the long averaging times associated with Raman lidar measurements, the method that is most adaptable to performance of high-resolution measurements of H_2O from an aircraft is the DIAL technique.[5] Thus all the current airborne lidar systems measure H_2O with the DIAL technique.[9,10] The NASA Langley Research Center's (LaRC) airborne H_2O DIAL system was designed to conduct mesoscale investigations of H_2O and aerosol distributions under diverse meteorological conditions during both daytime and nighttime operation.

Measurement Methodology

A comprehensive approach was taken in the H_2O DIAL research program to ensure that the airborne DIAL system would be capable of providing high-accuracy H_2O measurements over a large range of atmospheric conditions. A detailed error analysis of the DIAL technique for the measurement of H_2O profiles was performed, and this analysis included random errors caused by lidar signal uncertainties and systematic errors caused by uncertainties in our knowledge of the H_2O absorption cross section. Experimental measurements were also conducted to improve our knowledge of the H_2O line parameters.

H_2O Concentration Measurement

DIAL Technique

Because many authors have already presented thorough treatments of the DIAL technique,[11,12] only an overview of the theory is reviewed here. The DIAL procedure requires that one use high-energy, narrow-linewidth, tunable lasers to achieve accurate range-resolved gas measurements. One laser is tuned to an absorption line of the molecular species of interest (on-line), and the other is tuned to a nearby spectral region that has little or no absorption by the gas (off-line). The on-line and the off-line pulsed laser beams are transmitted through the atmosphere, and a portion of the laser radiation is backscattered by molecules and aerosols to a telescope receiver system that is colocated with the laser. The backscattered power from range R at the detector is given by

$$P(R) = P_0(c\tau/2)R^{-2}A\eta\beta(R) \times \exp\left\{\int_0^R 2|\sigma n(R) + k(R)|\mathrm{d}R\right\}, \quad (1)$$

where P_0 is the transmitted power, c is the velocity of light, τ is the laser-pulse duration, R is the range, A is the receiver area, η is the receiver–detector efficiency, $\beta(R)$ is the atmospheric volume backscatter coefficient, σ is the absorption cross section of the molecular species of interest, $n(R)$ is the number density profile of the gas, and $k(R)$ is the atmospheric extinction coefficient resulting from all other attenuation processes.

Provided that the on-line and the off-line transmitters are close in wavelength ($\Delta\lambda \leq 0.1$ nm), we can assume that $\beta_{on}(R) = \beta_{off}(R)$ and that $k_{on}(R) = k_{off}(R)$, and we can solve Eq. (1) for the number density profile of the gas:

$$n(R) = \frac{1}{2(R_2 - R_1)(\sigma_{on} - \sigma_{off})} \ln \frac{P_{off}(R_2)P_{on}(R_1)}{P_{off}(R_1)P_{on}(R_2)}, \quad (2)$$

where $R_2 - R_1$ is the range cell for the average gas concentration, $\sigma_{on} - \sigma_{off}$ is the differential absorption cross section for the two wavelengths, P_{on} is the power received from range R for the on-line wavelength, and P_{off} is the power received from range R for the off-line wavelength. One can then convert the number density profile to a volume (or mass) mixing ratio by dividing the gas number (or mass) density by the ambient atmospheric number (or mass) density.

DIAL Measurement Errors

Errors in the measurement of H_2O with the DIAL method arise from both random and systematic sources. A discussion of these measurement errors for DIAL systems is available in the literature,[13-15] and a detailed discussion of random and systematic errors for H_2O DIAL systems is given in Ref. 16. Random errors are caused by noise in the signal. Variability of the photon statistics in the lidar return signal, noise resulting from detector dark current, and noise in the background signal are the main sources of random error. One can minimize the random error associated with DIAL measurements by maximizing the signal-to-noise ratio (S/N). The S/N increase can be achieved in several ways, including an increase in laser-pulse energies or pulse repetition rates, an improvement in the optical throughput of the system, the use of a detector system with higher quantum efficiency or lower dark-current noise, and the selection of a narrow-band optical filter that rejects most of the day background light and retains high optical efficiency. Following acquisition of the lidar data, we minimize random errors in the DIAL measurement by averaging the data. As a first step in noise reduction, the signals are averaged by smoothing them along the range, followed by averaging of a number of lidar profiles to enhance the precision of the measurement. This averaging of signals also results in a reduction in vertical and horizontal resolution. Thus a trade-off is necessary to achieve a balance between spatial resolution and measurement precision (typically a vertical range resolution of 200–300 m and an averaging of 300–600 laser shot pairs are used in data reduction). Systematic errors in DIAL measurements are caused by both atmospheric and instrumental effects. The DIAL system presented here is designed and operated to minimize

the influences of systematic effects. Selection of the alexandrite on-line laser with a narrow linewidth and a high spectral purity, and its operation at the center of H_2O lines, ensures minimum influences in the DIAL measurement that are caused by the laser spectral distribution. The DIAL system is operated to avoid signal-overload effects, and the data analysis is restricted to regions that are not significantly influenced by signal overloads, signal nonlinearities, signal-digitization errors, and on–off signal-synchronization influences. The H_2O line selection ensures that negligible influence results from sensitivity of the H_2O cross section to uncertainity in the knowledge of atmospheric temperature. It is estimated that the sum of these systematic influences in cleaner regions of the lower troposphere will result in DIAL systematic errors of less than 5%.

H_2O Spectroscopy

Clearly, from Eq. (2), uncertainties in the knowledge of the gas absorption cross section can lead to errors in the DIAL measurements of gas profiles. Atmospheric influences on the effective cross section (i.e., the absorption cross section at the laser wavelength) are caused by the dependence of the absorption linewidth and the absorption line-center position on pressure and temperature and by the dependence of the line strength on temperature. A high-resolution spectroscopy experiment that incorporated a narrow-lindwidth tunable dye laser and two multipass absorption (White) cells with different pressure or temperature conditions has been used to provide measurements of H_2O absorption-line parameters in the 720-nm-wavelength region.[17,18] The use of the two multipass cells in parallel ensures that the results are insensitive to any laser-frequency drift during the measurement. Measurements of line strengths, pressure broadening, pressure-induced line shifts, and broadening and shift temperature dependences in the range 300–400 K were made. The pressure-shift coefficients in air were found to vary from line to line, and the average value was found to be -0.0170 cm^{-1}/atm. The temperature exponent for the air broadening was found to be J dependent, with the broader lines (i.e., low-J lines) having the higher exponent. The average exponent value was measured to be 0.67. The temperature-dependence exponent for the line shift in air was also found to be J dependent, but it showed the opposite behavior (i.e., the high-J lines had the higher exponents). The temperature exponent for the line shifting varied between 0.4 and 1.2.

Using these laboratory measurements, we accurately determined the effective differential absorption cross section for atmospheric H_2O, with an absolute error of 3–6%, for more than 120 H_2O absorption lines in the 720-nm region. These H_2O lines have a wide range of absorption cross sections and ground-state energies that can be selected to optimize the DIAL measurement according to the various atmospheric conditions encountered during the field experiments.

Scattering-Ratio Measurement

Along with the DIAL H_2O profile measurement, The DIAL system simultaneously provides information on the atmospheric aerosol distribution. An atmospheric scattering ratio is used to quantify the distribution of aerosols in the path of the laser beam. The scattering ratio is defined[11] as the ratio of the sum of the volume backscatter coefficients β for the molecular and the aerosol components of the return to the coefficient for the molecular signal only:

$$R(r) = \frac{\beta_m(r) + \beta_a(r)}{\beta_m(r)} = 1 + \frac{\beta_a(r)}{\beta_m(r)}. \qquad (3)$$

To determine the atmospheric scattering ratio, a measurement is first made in a clean region ($\beta_a \approx 0$) to establish the relative molecular scattering profile. We then calculate the calibration constant by taking the ratio of the clean-region lidar return signal to the National Meteorological Center (NMC) molecular density at that location. The calibration ratio is then used to normalize the NMC molecular density profile at any other location. This calculated molecular lidar return can be divided into the total lidar return to give the atmospheric scattering ratio.

Airborne H_2O DIAL System

In its present configuration,[9] the NASA airborne H_2O DIAL system uses advanced instrumentation and technologies to provide enhanced H_2O measurement capabilities over the previous dye-laser-based H_2O DIAL system.[19,20] The system has evolved over the past 5 years to include tunable solid-state laser technology; equipment for accurate wavelength positioning, stabilization, and monitoring; advanced data-acquisition and experiment-control electronics; high-throughput receiver optics; and solid-state detector technology. The airborne H_2O DIAL system consists of five major subsystems: the laser transmitters and transmission optics, the equipment for wavelength positioning and monitoring the receiver optics and detectors, the timing and control electronics, and the data-acquisition instrumentation. The laser transmitters and the transmission optics are contained, along with the wavelength-monitoring equipment, in a rigid structure that is bolted to the aircraft seat tracks. The receiver system is also attached to this structure, and it can be mounted for either nadir or zenith operation. Three dual aircraft racks house the data-acquisition and the experiment-control electronics, the laser power supplies and heat exchangers, and the wavelength-control electronics. A fourth rack, smaller than the dual racks, holds the two color printers used for real-time data output. A schematic of the airborne H_2O DIAL system in the NASA Wallops Flight Facility (WFF) Electra aircraft is shown in Fig. 1.

Laser Transmitters

Different laser systems are used to generate the on-line and the off-line wavelengths for the H_2O

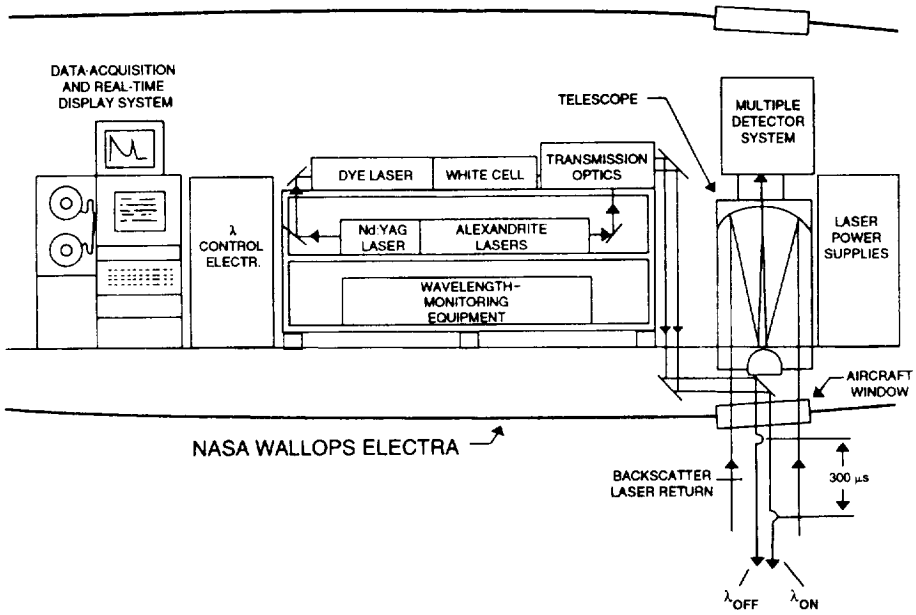

Fig. 1. Schematic diagram of the NASA LaRC airborne H_2O DIAL system.

DIAL measurement. A tunable, narrow-band alexandrite laser is used as the on-line transmitter to provide the requisite linewidth, wavelength stability, and spectral purity for accurate measurement of H_2O concentration. Because the spectral requirements for the off-line laser are less stringent than those for the on-line laser, an Nd:YAG laser-pumped dye laser is used to generate the unabsorbed wavelength.

On-Line Laser

The alexandrite laser used as the on-line transmitter (Fig. 2) is a custom-designed laser system developed by Allied Military Laser Products. A double-ellipse pump chamber contains two flashlamps and a 110 mm × 5 mm (length × diameter) alexandrite rod with antireflection-coated plano–plano ends. Because the alexandrite emission cross section increases with temperature, the laser rod is heated to 70 °C with a heat exchanger to optimize the laser gain. A separate cooling loop is used to operate the lamps at a lower temperature of 40 °C. The Fabry–Perot cavity that encloses the pump chamber is composed of a reflector with a 5-m-high radius of curvature and a 60%-reflectivity plano output coupler. This resonator cavity is Q switched with an acousto-optic device to produce a 200-ns pulse length at a rate of 10 Hz. The laser wavelength and linewidth are controlled with a birefringent tuner for coarse control and a pair of Fabry–Perot étalons for fine control. The birefringent tuner, which consists of a stack of five quartz plates in a ratio of 1:2:2:10:10, is angle tuned with a stepper motor. A 1-mm-thick plate of fused silica with 30%-reflectivity coatings is used for the low-resolution étalon. This element serves as an order selector for the high-resolution étalon and is also angle tuned by a stepper motor. The high-resolution étalon is a 1-cm air-spaced Fabry–Perot étalon that consists of two wedged, fused silica plates with 30%-reflectivity coatings on the inside surfaces and antireflection coatings on the external surfaces. We tune this element by varying the spacing of the plates with piezoelectric ceramics. Synchronous scanning

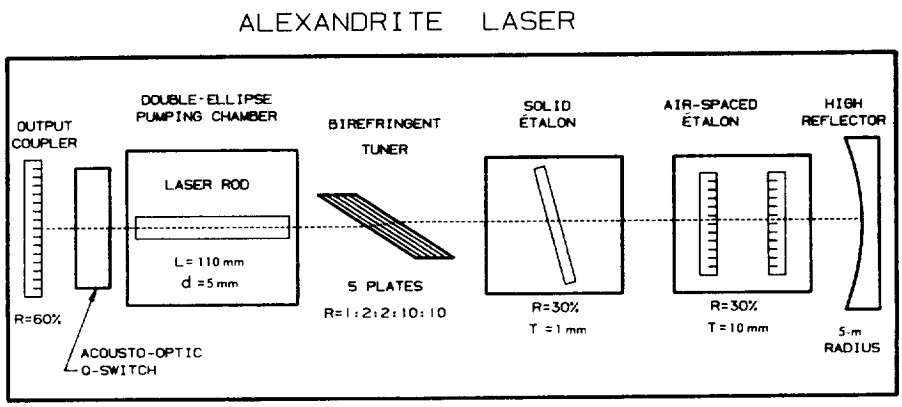

Fig. 2. Optical configuration of the alexandrite laser cavity.

of the laser over a sufficient wavelength interval without mode hopping requires that the free spectral range ratio between the two étalons be very close to a half-integer value. This ratio is adjusted by use of a scanning single-longitudinal-mode ring dye laser as a calibration source.[21] The three intracavity tuning elements together provide an output linewidth of less than 1.1 pm (FWHM). They can be synchronously scanned through a microprocessor-controlled routine to vary the laser wavelength continuously over a 150-pm region located anywhere in the 725–785-nm tuning range of the laser. Because the large number of coated intracavity elements, the output pulse energy of the laser is limited to 30 mJ to minimize the possibility of optical damage.

For accurate DIAL measurements, the laser line must be nearly monochromatic with respect to the absorption line; i.e., it must have high spectral purity and a narrow linewidth. Spectral purity is defined as the percentage of laser energy transmitted within a specific spectral interval relative to the total transmitted laser energy. For the H_2O lines in the 730-nm region, the spectral purity must be $>99\%$ to achieve high-accuracy H_2O measurements.[16] In addition to high spectral purity, the laser linewidth must be small compared with the linewidth of the H_2O absorption feature. Finite laser linewidths lead to uncertainties in the knowledge of the absorption cross section and cause systematic errors in the DIAL measurements of the H_2O profiles.[15,16]

The spectral properties of the alexandrite laser were measured with a multipass absorption cell and a ratiometric energy meter.[22,23] These multipass-cell transmission values indicated that the spectral purity of the alexandrite laser was $\geq 99.85\%$. To determine the influence of the finite laser linewidth, measurements of the effective absorption cross section were made for different values of the absorption linewidths of H_2O and oxygen. For absorption linewidths greater than 4 pm (FWHM), which correspond to altitudes below 10 km, the cross section is within 1% of the cross section calculated from spectroscopic data.[18,22,23] Therefore, under these conditions, the alexandrite laser can be considered to be monochromatic with respect to the H_2O absorption line.

In addition to having a monochromatic spectral distribution, if the line-center absorption cross section is used in the data-reduction process, a precise positioning of the laser wavelength relative to the H_2O absorption line center is required for accurate measurement of H_2O concentration. To obtain a DIAL H_2O measurement error of less than 5% at altitudes below 5 km, the laser-wavelength deviation from the center of the absorption line must be less than ± 0.8 pm, including initial positioning uncertainty, shot-to-shot wavelength jitter, and long-term wavelength drift.[16] Without additional wavelength stabilization of the alexandrite laser, however, mode hopping and wavelength drifts as large as 3 pm/h have been observed in a controlled laboratory environment. Consequently, a stabilization device was designed and implemented to maintain the required spectral characteristics despite the pressure, humidity, and temperature variations and the mechanical vibrations inherent in an aircraft environment.[22,23]

A Laboratory for Science model 200 wavelength-stabilized cw He–Ne laser is used as an external absolute reference to stabilize the optical thickness of the two Fabry–Perot étalons actively. We generate two error signals by comparing the output intensity of the He–Ne laser with the intensities of the He–Ne laser beam that reflects from the air-gap étalon and that transmits through the solid étalon. The angle of the He–Ne beam through each étalon is adjusted so that the He–Ne laser wavelength corresponds to the half-maximum of each of the Fabry–Perot transmission modes. At this point there is a maximum sensitivity to changes in the optical thickness of the étalons. The three intensity levels are digitized and sampled by a computer, and the computer creates the appropriate correction voltages, which are applied to the étalon controllers. Using an absorption feature of oxygen contained in a multipass cell as a reference, a long-term (≈ 1.5 h) laser drift of less than 0.7 pm relative to the absorption-line center was observed.

Off-Line Laser

As shown in Fig. 3, the off-line laser wavelength is generated by use of a Quantel model 482 frequency-doubled Nd:YAG laser to pump a Jobin–Yvon model HP-HR tunable dye laser.[19,20,24] The Nd:YAG laser oscillator uses a stable resonator configuration to produce a TEM_{00} transverse-mode output beam at 1.06 μm, with a pulse length of 12 ns. After being up-collimated by a telescope, the oscillator beam is passed through two amplifiers, giving it an output energy of 1 J/pulse at a repetition rate of 10 Hz. For frequency doubling to 532 nm, an angle-tuned, temperature-stabilized KDP-II crystal with 40% efficiency is used to generate 400 mJ/pulse. Two dichroic beam splitters are used to separate the visible and the infrared wavelengths and to direct the green pump beam into the dye laser.

To produce the high-energy, narrow-linewidth output pulses required for accurate DIAL measurements, the dye laser also uses an oscillator–amplifier configuration. Narrow-linewidth operation is achieved with incorporation of a Littrow-mounted holographic grating in the oscillator cavity. In combination with an intracavity Pellin–Broca prism, the grating (2400 lines/mm) produces a linewidth of less than 15 pm, which is adequate to satisfy the off-line laser requirements. The line-narrowed output from the oscillator is amplified in three stages: the first stage is a preamplifier that operates below saturation, and the final two stages are amplifiers that operate near saturation. By sufficient saturation of the amplifiers, the input energy is efficiently transferred to the narrow-band portion of the laser beam, and amplified spontaneous emission is minimized.[25] The amplified spontaneous emission generated by the preamplifier is suppressed by two Pellin–Broca prisms

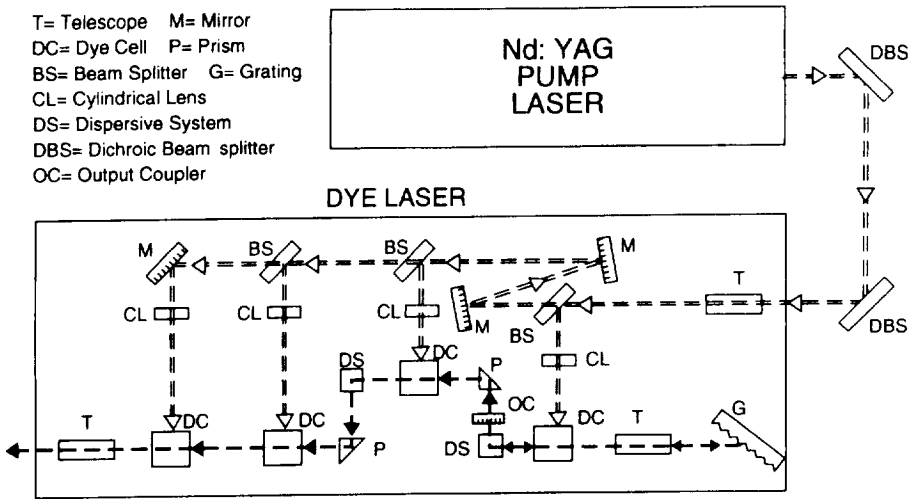

Fig. 3. Optical configuration of the Nd:YAG and the dye lasers.

placed between the preamplifier and the first amplifier. The dye solution used for operation near 730 nm is Exciton LDS-751 in methanol. With this dye solution the laser produces an output energy of 60 mJ, which corresponds to a conversion efficiency of 15%. To permit the use of the same detection system in the receiver for the on-line and the off-line lidar returns, the two laser systems are fired with 300-μs separation. This is close enough to sample the same atmosphere with the laser beams but far enough apart to have independent lidar return signals. In addition, even though the 200-ns pulse length of the flashlamp-pumped alexandrite laser is much longer than the 12-ns pulse of the dye laser, this can be compensated for in the data-processing procedure. Performance characteristics of both the on-line and the off-line airborne H_2O DIAL laser transmitters are summarized in Table 1, and a block diagram of the laser transmitters, wavelength-control equipment, and spectral-monitoring equipment is presented in Fig. 4.

Transmission Optics

Before they are transmitted into the atmosphere, the alexandrite and the dye-laser output beams pass through various optical components for attenuation, evaluation, and steering. First, as a result of ground observer eye safety considerations during nadir operation, each beam is sent through a variable attenuator consisting of two polarizers with a $\lambda/2$ plate between them. Depending on aircraft altitude, we adjust the output beam energies with the attenuators to achieve a combined radiant exposure at ground level that is below the maximum permissible exposure value as determined by the American National Standards Institute.[26] Energy monitors, which use less than 2% of the output laser energy, are mounted after the attenuators, and the shot-to-shot output energy is measured and recorded. The beams are then reflected off of separate mirrors held in motorized gimbal mounts for independent optimization of each beam in the receiver field of view. Both beams are finally reflected off a single mirror mounted behind the telescope secondary and transmitted coaxially with the receiver telescope into the atmosphere. The beams are completely enclosed in baffles until they reach the aircraft window to prevent scattered light from entering the telescope. Beam steering and energy attenuation are accomplished remotely from the data-acquisition system.

Monitoring Instrumentation

A McPherson model 2051 spectrometer and a Spectra Physics model LO-3 absorption cell (see Fig. 4) are used to position the on-line transmitter wavelength at the center of an H_2O line and to monitor the performance of the laser during flight. The 1-m spectrometer incorporates a 1200 lines/mm holo-

Table 1. Airborne H_2O DIAL Transmitter Characteristics

Characteristic	Value
On-Line	
Alexandrite laser	
(Allied model 407000)	
Wavelength	725–780 nm
Pulse energy	30 mJ
Pulse length	200 ns
Repetition rate	10 Hz
Linewidth	1.1 pm
Spectral purity	> 99.85%
Wavelength stability	0.7 pm
Wavelength jitter	< ±0.5 pm
Off-Line	
Nd:YAG laser	
(Quantel model YG482)	
Wavelength	532 nm
Pulse energy	400 mJ
Pulse length	15 ns
Repetition rate	10 Hz
Dye laser	
(Jobin–Yvon model HP-HR)	
Wavelength	726–730 nm
Pulse energy	30 mJ
Linewidth	~ 15 pm

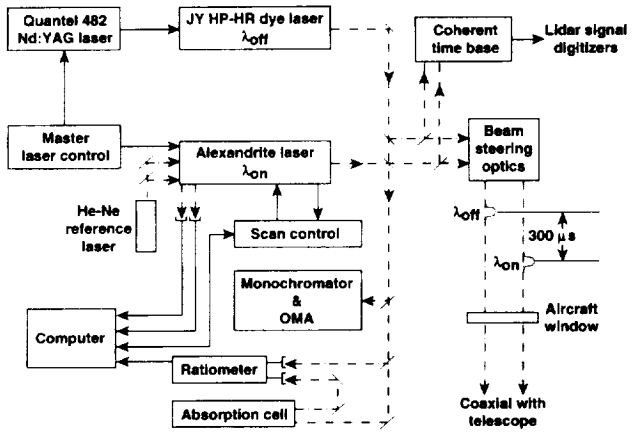

Fig. 4. Block diagram of the H_2O DIAL laser transmitter subsystem including laser transmitters, wavelength-control equipment, and spectral-monitoring instruments. JY, Jobin–Young, OMA, optical multichannel analyzer.

graphic grating in a Czerny–Turner optical configuration to produce a linear dispersion of approximately 0.7 nm/mm at 730 nm. A Princeton Applied Research optical multichannel analyzer (OMA), which consists of a model 1205D linear array detector head attached to the spectrometer and a model 1205A control unit, is used to evaluate the spectral characteristics of the output beam. The detector has a pixel spacing of 25 μm, which corresponds to a wavelength dispersion of 17.5 pm/pixel and provides a wavelength-positioning accuracy of better than ±20 pm.

The multipass absorption cell is of stainless-steel construction and has a heating jacket for high-temperature operation. The cell mirrors have dielectric coatings with >99% reflectivity over the range 725–790 nm. During operation, the cell is evacuated, heated to 60 °C, and filled with approximately 40 Torr of pure H_2O. Because the saturation vapor pressure at 60 °C is 150 Torr, the risk of condensation on the mirrors is minimized. A Laser Precision model RJ7200 ratiometric energy meter with model RJP 765 silicon probes is used to measure the amount of absorption through the multipass cell. A stability test was performed to determine the ratiometer precision associated with this type of measurement. The ratiometer precision, defined as the variation in the absorption-cell transmission divided by the average absorption-cell transmission, was determined to be 1% when we evaluated the reproducibility of the beam transmission through the evacuated absorption cell with the laser set at a fixed wavelength.[23] Taking into account the ratiometer precision, there is sufficient optical depth, with an H_2O pressure of 40 Torr and a path length of 100 m in the cell, to position the alexandrite wavelength accurately at the center of H_2O lines having absorption cross sections greater than 4×10^{-24} cm^2/molecule.

Thus the procedure implemented to optimize the alexandrite output on an H_2O line is first to set the wavelength as close as possible to the selected H_2O line by use of the spectrometer–OMA, with an atomic vapor lamp as a reference. Next, while observing the absorption-cell transmission on the ratiometer readout, we vary the laser wavelength by synchronously scanning the intracavity tuning elements. When the maximum absorption through the multipass cell is detected, the laser wavelength is locked on the H_2O line by use of the stabilization device described above. Using the spectrometer–OMA combination, we set the off-line wavelength between 60 and 100 pm from the on-line wavelength in a region free of other absorption features.

Both the spectrometer–OMA combination and the absorption cell are also used for real-time monitoring of the alexandrite spectral characteristics during flight operations. A small portion of the output is kicked off and sent through fiber optics to the spectrometer. Mode hops between adjacent thin étalon modes (free spectral range 180 pm) that result from a drift of the birefringent tuner or of the étalon itself can be seen on the OMA display. A beam splitter is also placed in the beam to reflect 4% of the output into the absorption cell. Thus any drift in wavelength that is caused by a variation in the optical path through the air-spaced étalon will be immediately detected by the ratiometer. In addition, a shot-to-shot measurement of the effective absorption cross section in the absorption cell can be recorded.

Receiver System

Figure 5 shows the present optical configuration of the receiver system. The receiver system incorporates a 36-cm-diameter Celestron model C-14 telescope with Schmidt–Cassegrain optics to collect the backscattered laser light and focus it into the detector package. An iris placed in the telescope focal plane acts as a variable field stop for adjusting the field of view of the receiver. The field of view is normally set at 2 mrad to contain greater than 97% of the energy in the approximately 1.5-mrad-divergence laser beam. In addition to having interchangeable detectors, the detector package contains optics for beam collimation, filtering, and focusing. After passing through

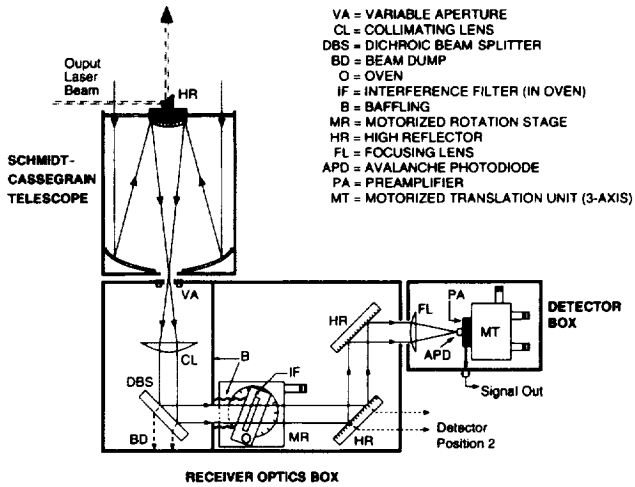

Fig. 5. Optical configuration of the H_2O DIAL receiver system.

the field stop, the laser light is collimated by a 100-mm-focal-length lens and prefiltered with a dichroic beam splitter. The lidar signals are then transmitted through an interference filter to reject background light and any Raman scattered laser light further.[27] After it is transmitted through the filter, the laser light can be directed to two possible detector positions. In addition, the available return power can be split between a near-field detector with low gain and a far-field detector with high gain to improve the dynamic range of the measurement.[24] Various filter and detector configurations were used in flight tests conducted during the field measurement campaigns, and substantial improvements were implemented between each field deployment. Table 2 lists the important characteristics of the airborne H_2O DIAL receiver system.

Receiver Filters

During daytime operation, a 0.4-nm-bandwidth (FWHM) filter is required for high solar-background rejection. The daytime filter (Spectro-Film 7289/3-4 SF) used during the 1989 and 1990 field measurements had a relatively low transmission of 33%. However, a new filter (Andover ANDV1551) with a transmission of 48% was acquired before the 1991 flight tests. This represents a receiver system efficiency increase of 45% and a resulting measurement S/N increase of 20%. The increase in S/N is reflected in the 1991 H_2O data, which required substantially less signal shot averaging than the 1989–1990 data. At night, a higher-transmission 1-nm-bandwidth filter (Spectro-Film 7289/10 SF) replaces the daytime filter, beause only the Raman-backscattered component needs to be blocked. In addition, nighttime measurements can be made with no filter in place if corrections are made for the Raman return signal, which is approximately 3% of the Rayleigh return signal.[27] The filters are placed in an oven and heated to 40 °C to stabilize their transmission peaks thermally at the on-line wavelength. The H_2O lines in a 4-nm-wavelength range can be achieved with each filter by use of angle tuning with a motorized encoder rotation stage.

Receiver Detectors

During the field deployments, a photomultiplier tube (PMT) and an avalanche photodiode (APD) were incorporated as detectors for both daytime and nighttime measurements in diverse meteorological conditions to determine which detector exhibited optimum performance in the system. The choice of a detector is very important because it can influence both system throughput and dark current. An APD detector provides high quantum efficiency, but it has increased noise because of high dark current and a large excess-noise factor.[16] Compared with an APD, a PMT has lower quantum efficiency, but at the same time the PMT has a lower dark current and a lower excess-noise factor. As has been discussed in the literature,[16,28,29] the APD is more suitable for DIAL measurements in cases in which signals are strong compared with the detector dark current, and a PMT is more suitable for measurements in low-signal regimes.

The RCA model 7265 PMT has an enhanced S-20 photocathode for improved operation in the red and the near-infrared regions of the spectrum. The APD module includes a 1.5-mm-diameter RCA model C30955E APD and its preamplifier, motorized encoder translation stages to optimize the position of the APD in the field of view, and focusing optics to image the field stop on the APD surface. The APD data indicated a much higher measurement S/N, thus leading to higher precision and longer-range measurements with this detector. This conclusion is evident from Fig. 6, which shows a comparison of the measured H_2O mass mixing ratios (M), the mixing ratio standard deviation (σ), and the measurement signal-to-noise ratio (M/σ) from a nighttime flight test on 18 April, 1991. We accomplished the detector comparison by conducting measurements on a specific flight path with the PMT and, after changing detectors during the turn, retracing the same path for measurements with the APD. The data shown in Fig. 6 have been calculated with a 210-m vertical range cell size and averaged in the horizontal direction over approximately 12 km. The S/N plots clearly indicate the superior performance of the APD over the entire altitude range, with the exception of the final 300 m of the measurement. Improvement over the PMT is expected to be even greater during

Table 2. Airborne H_2O DIAL Receiver Characteristics

Characteristic	Value	
Receiver area	0.1 m^2	
Field of view	1.5 mrad	
Filter bandwidth	0.4 nm	
Filter transmission	48%	
Optical efficiency	34%	
Detector type	PMT	APD
Quantum efficiency	3.9%	85%
Total efficiency	1.3%	29%

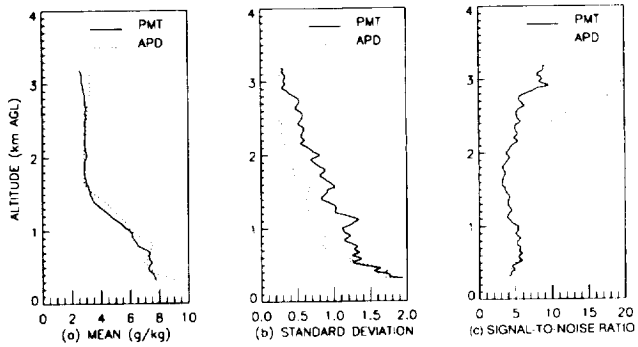

Fig. 6. Performance comparison of the APD and the PMT detectors from a flight on 18 April 1991. The plots show (a) the measured mixing ratio profiles, (b) the mixing ratio standard deviation profiles, and (c) the mixing ratio S/N profiles. AGL, above ground level.

daytime operation because the PMT S/N is degraded by background radiation, whereas the APD S/N is still dark current limited.[29]

Timing, Control, and Signal-Processing Electronics

As mentioned above, the on-line and the off-line laser pulses are transmitted sequentially, with a temporal separation of 300 μs. This approach reduces receiver system complexity by eliminating the need to separate the DIAL wavelengths spectrally. However, the simplification of the receiver system is at the expense of increased complexity in the design of the timing and control electronics.

The inherent characteristics of the acousto-optic *Q* switch used in the alexandrite laser further complicate the requirements of the timing and the control functions. For example, the output from the alexandrite occurs approximately 4.7 μs after the lase command is issued and has a 150-ns jitter, whereas the output pulse from the Nd:YAG system occurs 0.23 μs after its lase command, with a jitter of only 3 ns.

The most important factor in the timing methodology is the synchronization of the sequential laser firing with the return signal digitization. To fulfill the timing requirements, a master control unit was developed to control laser flashlamp firing, lase fire command, and PMT gating with a precision of ±10 ns. In addition, a lase-coherent time base was designed to provide a digitizer trigger that is synchronized with the actual laser firing, which is detected with fiber-optic pickup by use of a fast photodiode incorporated in the time base. The time base of the digitizer is stopped and restarted with the correct phase relative to the time of the laser firing for both the on-line and the off-line laser pulses. This phase correction was found to be necessary because an improper delay between the on and the off signals can distort the DIAL-measured profile in regions of strong aerosol gradients.[30]

The lase-coherent trigger to the digitizer is generated at the time of the alexandrite laser firing, and any timing jitter between the alexandrite and the Nd:YAG laser pulses would result in an apparent desynchronization of the dye-laser return in the digitizer memory. Because the alexandrite laser does have a significant amount of jitter associated with it, a modification was implemented to create a precision delay in the Nd:YAG output referenced to the on-line laser pulse by use of a Data Design model DG11A digital delay generator. Other features include phase-aligned, precision-delayed lase markers summed with the return signals and line-locked firing-rate logic that minimizes 60-Hz drift in the dc offset.

When a PMT is used as the detector in the receiver system, it is gated on by a transistor–transistor logic pulse with an adjustable time delay after each laser pulse is transmitted. PMT gain is controlled by manual ajdustment of the high voltage supplied to the PMT dynode network. The APD, however, is a nongated detector with fixed gain. The return signals are filtered (2.5-MHz bandwidth) and amplified by a factor of 10 with a Digital Signal Processing (DSP) model 1020 amplifier. The signals are then digitized at 10 MHz by use of a 12-bit DSP model 2112S transient recorder with averaging memory. Both the on-line and the off-line DIAL returns are processed sequentially during a 4096-Word sweep of the digitizer. Each sweep can then be stored and summed in the averaging memory. Typically, 15 sweeps are summed before they are transferred to the host computer. The digitizer and the amplifier are interfaced to a computer automated measurement and control (CAMAC) crate, and certain functions, such as the number of sweeps summed, are directly programmable from the computer.

Data-Acquisition System

The DIAL Data Acquisition System (DAS) is an advanced version of the system described in Ref. 31. The DAS occupies a standard aircraft double rack with digitizers, control electronics, and PMT power supplies in one half and the computers and peripherals in the other half. The digitizer and the amplifier are mounted in a CAMAC crate, and they communicate with the rest of the data system through a Kinetics System model 3922 crate controller. Through this crate controller the computer system is able to set up various options as well as initialize and enable the digitizer. When the programmed number of sweeps has been accomplished, an interrupt is generated by the digitizer, and the data are then transferred from the averaging memory to the host computer through the crate controller. Other inputs to the computer system include laser energies, aircraft position data (latitude and longitude information from the aircraft inertial navigation system), pressure, total temperature, dew-point temperatures, and absorption-cell ratiometer readings. Laser energies are detected and converted from analog to digital through a custom-designed energy monitor system. The aircraft position data are in an ARINC-561 format and are decoded by custom-designed electronics. Energies and navigation data are transferred to the host computer through two 16-bit parallel interfaces. Pressure, total temperature, and dew point from two instruments are converted from analog to digital signals, sent through light pipes from the front of the aircraft to the DIAL system at the rear, and transferred to the computer through a third parallel interface. The ratiometer reading of the absorption-cell transmission is converted to RS232 format and interfaced to the computer through a four-channel serial input–output CAMAC module.

The DIAL DAS is based on two Digital Equipment Corporation (DEC) PDP 11/73 processors and one MDB JFEP-11 front-end processor. Each PDP has 128 kWords of 16-bit memory, although only 28 kWords of memory is available for resident programming. The overall flow chart for the DIAL DAS is shown in Fig. 7. In general, all data acquisition and storage are performed by the PDP at the left in Fig. 7

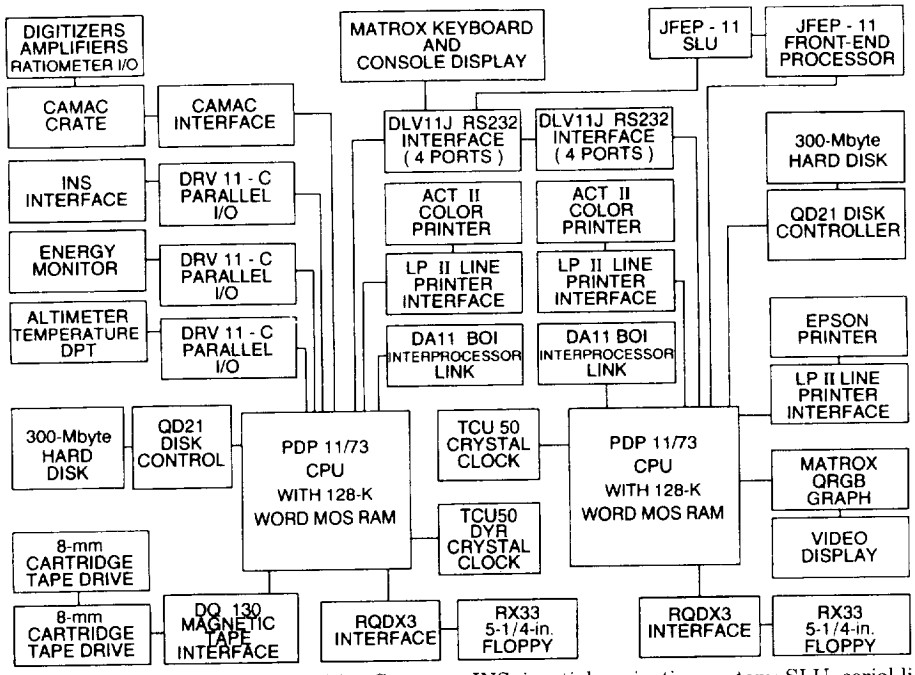

Fig. 7. Block diagram of the H_2O DIAL Data Acquisition System. INS, inertial navigation system; SLU, serial line unit; MOS, master operating system.

(PDP-1), whereas all data display and analysis are performed by the PDP at the right in Fig. 7 (PDP-2). The JFEP-11 is housed in PDP-2 and has 256 kWords of memory, of which 128 kWords can be shared with the host computer. The DEC RT11-SJ operating system is used for software development. The operating system and the DIAL software are stored on and retrieved from 300-Mbyte hard disks. Also available on each PDP is a 5-1/4-in. floppy disk drive for hard disk backup. These floppy disks are also used for data input to the DIAL DAS from external computers.

PDP-1 acts as the master computer through which the operator communicates with PDP-2 and the JFEP. The operator communicates with the processors through a Matrox CTM-300 smart keyboard, and input–output is echoed on a small black and white monitor. The keyboard interfaces to PDP-1 through the console port of a four-port serial line interface (RS232). A second port of this interface connects to PDP-2, and a third port connects to the JFEP serial line unit.

The DIAL DAS operating system software consists of three programs that run concurrently on the two PDP processors and on the JFEP processor. When the DIAL master program is being loaded on PDP-1, commands are automatically generated to load and run appropriate programs on the other two processors. In the data-acquisition mode, PDP-1 will collect the digitizer data, the supplemental information mentioned above, and the time and date from a crystal clock into one long data buffer. This buffer can represent anywhere from 1 to 65536 laser pairs summed in the digitizer averaging memory. Once the digitizers achieve the selected number of sweeps, an interrupt is sent to alert PDP-1. The auxilliary information is then attached in the form of a buffer header, and the entire buffer is then recorded on 8-mm cartridge tape in binary format. The data buffer and a table of display options are then sent to PDP-2 through a direct-memory-access interprocessor link. The data buffer and the display table are shared between PDP-2 and the JFEP through dual-ported memory.

The user controls data-acquisition and display options by keying in commands specifically designed for this DIAL system. The command structure format provides a fast update of user-selected options. Function keys are defined for some of the more frequently used commands.

As stated above, PDP-1 is mainly dedicated to data acquisition and storage and to communication with the operator. Additionally, if a particular display option is selected, PDP-1 will process the data for aerosol information and compute either the relative aerosol scattering ratio or the total aerosol scattering ratio. The aerosol profiles are then color coded and presented as a function of time and altitude on one of the ACT II inkjet printers.

The main function of the second PDP is to perform selected analysis options for display on a black and white monitor through a graphics display controller. The display modes are designed to provide diagnostic tools, feedback on beam optimization, and results of calculations of aerosol and H_2O profiles. The most basic mode of display shows the returns from both lasers in an overlapped manner as a function of range. This display is used to observe signal levels during beam steering and beam optimization. The operator may elect to display only one of the returns, subtract

the background, smooth the return (by use of a running average), correct for range-squared dependence, normalize the return for laser energy, and average successive returns. Another display mode shows the relative aerosol scattering profile as a function of altitude with smoothing and averaging options. One can also calculate scattering ratios in this mode by specifying an altitude at which to normalize the lidar return to a model molecular number density profile. A H_2O mixing ratio profile can be calculated from each DIAL signal pair and successive profiles can be averaged to improve the measurement statistics. The updating average can be displayed as a function of altitude with range-cell size, smoothing, and averaging options.

A final display mode is implemented during spiral ascents and descents. The H_2O mixing ratios are calculated from *in situ* dew-point measurements and plotted as a function of altitude. These profiles can then be compared with inflight DIAL profiles obtained over the spiral point to provide validation of the DIAL system. Any screen display can be captured at any time and plotted with a dot matrix printer. Because the screen is stored in memory before plotting, there is only a brief pause before the screen update proceeds.

PDP-2 sends the DIAL returns to the JFEP. The JFEP stores a running average of DIAL returns and computes the DIAL calculation on that average to obtain a H_2O mixing ratio profile. Each profile is then returned to PDP-2, color coded for magnitude, and plotted on an ACT II inkjet printer as a function of altitude, time, and position. Real-time color cross sections of H_2O mixing ratios and aerosol scattering ratios are produced simultaneously by the H_2O DIAL DAS.

Field Measurements

During 1989–1991, the H_2O DIAL system was deployed to NASA WFF for three separate flight-test experiments. Preliminary engineering flights were performed in July 1989 to complete system shakedown and to assess system airborne operational reliability.[32] During March 1990 and April 1991, additional flight tests were conducted in a variety of meteorological conditions to verify the performance of the system and to establish the accuracy of the DIAL-measured H_2O profiles.[9,33] Included in these engineering and data flights were numerous intercomparison measurements taken with onboard dew-point hygrometers and H_2O radiosondes launched from both NASA LaRC and NASA WFF. Between each of the field deployments, many modifications were implemented to improve system performance and to automate system operation in flight further.

In Situ Instruments

Two dew-point hygrometers were used on the NASA WFF Electra aircraft to obtain *in situ* H_2O measurements: the EG&G model 137-C3 aircraft hygrometer and the modified EG&G model 300 microprocessor-controlled hygrometer. Both instruments use the chilled-mirror dew-point condensation principle to determine the H_2O concentration outside the aircraft. Details of this technique and of the operation of an EG&G 137-C3 hygrometer in aircraft field measurements can be found in Ref. 34. This unit incorporates a model S10 aircraft-mounted sensor head with a sampling probe designed to provide a static pressure sample at the correct mass flow rate across the chilled mirror. The model 300 hygrometer, on the other hand, is a laboratory unit, and we had to modify its model 53 sensor head by implementing a sampling probe for airborne operation. A major advantage of this instrument is the application of microprocessors and digital techniques to control the servoloop that maintains dew or frost in equilibrium on the mirror surface in the sensor. This approach leads to greater accuracy as well as the ability to operate effectively at lower dew points. The accuracy of the model 300 hygrometer is specified as ± 0.2 °C, whereas the accuracy of the model 137-C3 hygrometer is stated to be ± 0.5 °C. Conversion of the vapor pressures, determined with the dew-point temperature measurements, to H_2O mixing ratios is accomplished by making simultaneous measurements of the atmospheric pressure. *In situ* H_2O mixing ratio profiles were obtained with the dew-point hygrometers by spiraling the Electra down to a minimum altitude of 152.4 m at approximately 304.8 m/min.

Other *in situ* intercomparison profiles were acquired by H_2O radiosondes launched from ground stations located at NASA LaRC and NASA WFF. The balloons were released approximately 10 min before overflight by ground personnel who were in radio contact. Because the balloons typically ascend at approximately 200 m/min, this timing places the sonde at the center of the DIAL measurement altitude range when the plane is overhead (neglecting horizontal movement resulting from winds). The radiosonde package used for these measurements was the Vaisala model RS80, which incorporates solid-state thin-film capacitor sensing technology. This type of sonde was chosen because of its sensitivity and accuracy at relative humidity values below 20% as compared with the carbon element hygristor technique used in other packages.[35] Numerous overflights of NASA WFF and NASA LaRC were conducted to provide ample opportunity for DIAL–radiosonde comparisons. In addition, a standard landing procedure was used at NASA WFF, first to overfly the facility to obtain a DIAL profile and then to spiral the aircraft down while simultaneously launching a H_2O radiosonde. This landing procedure allowed us to intercompare all three H_2O profile measurement techniques.

System Parameters

Two H_2O absorption lines near 730 nm were used for the majority of the DIAL measurements. The stronger line, located at 728.7379 nm, has an absorption

cross section of 46.0×10^{-24} cm^2/molecule at ground level. This line was used extensively in the flight tests because of the ability to make high-accuracy measurements from 4 km to the surface over a broad range of meteorological conditions. The second line, with an absorption cross section of 21.6×10^{-24} cm^2/molecule at 1 atm, provides approximately a factor-of-2 decrease in the optical depth over the range cell compared with the stronger line. Measurements from higher altitudes and at elevated humidity levels required that we use this weaker line, which is located at 728.8126 nm. These two H_2O absorption lines were chosen for three primary reasons: (1) The receiver daytime filter center wavelength for light at normal incidence is 729.2 nm; (2) errors resulting from temperature sensitivity are small because both lines have lower energy levels in the temperature-insensitive range for mixing ratio measurements[36]; and (3) the lines are isolated, thus minimizing the errors caused by overlapping from adjacent lines and facilitating the positioning of the off-line wavelength. The dye-laser wavelength was placed at approximately 728.90 nm when the weaker line was used and at approximately 728.65 nm when the stronger line was used. In addition to providing the off-line laser return for the DIAL measurement, the dye-laser backscattered signal is also used to produce the atmospheric scattering-ratio profile.

Data Analysis

The postmission data analysis was done with a Microvax II computer. The data were first edited by rejection of shots resulting from poor laser energy or signals that were attenuated by strong near-field clouds to ensure that quality lidar return signals were used in DIAL calculations. The on-line and the off-line signal profiles were altitude aligned by shifting them to compensate for any slight difference in the altitude registering caused by a relative laser-firing delay. The data were background subtracted to remove the signal bias resulting from the daylight and the detector dark current. The signal profiles used in the calculations were limited to the region between the range past the full detector turn-on and the ground return or the cloud saturation point. Because of the difference in pulse lengths of the on-line and the off-line laser signals, the smoothing intervals of the two signals were adjusted to ensure an equivalent 300-m running sampling interval (vertical range) for DIAL calculations. The effective H_2O absorption cross-section altitude profile was calculated with the Voigt profile representation of the line shape,[37] spectroscopic parameters of the H_2O line, and the standard atmospheric model. This effective absorption cross-section profile is then used to calculate the H_2O number density profile by use of the DIAL equation [Eq. (2)]. The lidar returns used for the DIAL calculations were collected by use of shot accumulation times of 1 s onboard the aircraft. The 1991 data were further smoothed by use of a horizontal average of 6 km ($\approx$1 min), and for the 1990 data a variable horizontal interval that ranged from 6 km near the aircraft altitude to 30 km near the ground was required for the data to retain a good S/N over the entire altitude range. The DIAL-derived H_2O number density profile was converted to a mixing ratio profile by use of a midlatitude atmospheric model, and the error bars in the profile plots correspond to the standard error of the average H_2O profile.

Experimental Data

In Fig. 8 we show an example of a DIAL H_2O mixing ratio profile measured off the Virigina coast during a flight over the Atlantic Ocean on the night of 15 March 1990. The stronger H_2O absorption line was used during this flight, and the range cell applied to the return signals was 210 m. This profile represents an average of 600 shots, which corresponds to a horizontal resolution of approximately 10 km at the speed of the Electra. In Fig. 8 the DIAL plot is compared with the profiles generated by the two dew-point hygrometers as the plane spiraled down toward the water. The curves shown in Fig. 8 indicate very good agreement between the lidar-derived H_2O distribution and the *in situ* measurements, both in the absolute amount and in the vertical structure of H_2O. These data are consistent with the high H_2O levels and the shallow depth (typically $<$800 m) expected for a marine mixed layer. The higher peak value indicated by the EG&G 300 hygrometer in the layer located at 600 m may be partially the result of an overshoot problem associated with the instrument.

A flight was conducted on 22 March 1990 to demonstrate the daytime measurement capabilities of the system. As a result of the low levels of humidity measured at the WFF ground station that morning, the stronger line was again chosen for this

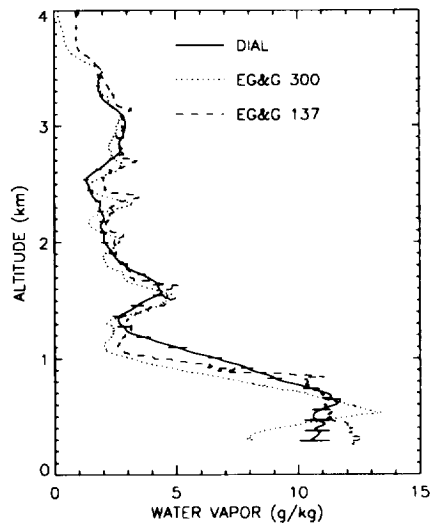

Fig. 8. Comparison of the DIAL and the DPT (dew-point hygrometer) H_2O volume mixing ratio (parts in 10^3) profiles at a location appproximately 125 km east of the Virginia coast during a nighttime flight on 15 March 1990.

flight test. Figure 9 presents an afternoon set of measurements over Emporia, Virginia. Because of the significant variations in the boundary layer, only the EG&G 300 hygrometer plot is shown for clarity. The difference between the DIAL and the dew-point-hygrometer profiles is $< 10\%$ over the entire range of the measurements. This agreement with measurements made with *in situ* probes is typical for the DIAL system. These results clearly show the ability of the DIAL system to make accurate, high-resolution measurements of large variations in the vertical distribution of H_2O.

After the Electra returned to flight altitude (4 km) above Emporia, we flew from Emporia to a point approximately 120 km off the coast of Virginia and observed the transition from a continental mixed layer to a marine mixed layer. Cross sections of the aerosol and the H_2O distributions encountered on this flight path are shown in Figs. 10(a) and 10(b), respectively. A 300-m range cell was used, and a horizontal average that varied with altitude was applied to the H_2O data to ensure that the ratio of the standard deviation to the mean of the horizontal values was $\leq 10\%$. The aircraft crossed the coast at 14:43 h local standard time (LST), and the measured aerosol and H_2O distributions clearly show the decrease in the mixed layer depth from approximately 1.7 km over land to less than 1 km over water. Increased H_2O concentrations can be seen near the coast in the continental mixed layer as a result of the daytime seabreeze circulation, and H_2O is seen to be positively correlated with aerosol loading. These airborne DIAL measurements show the detailed H_2O and aerosol structures that occur in the free troposphere and in the mixed layer over different land and marine regimes.

At the end of the 22 March flight test, an overflight and spiral descent were performed at NASA WFF before landing the aircraft. This procedure provided

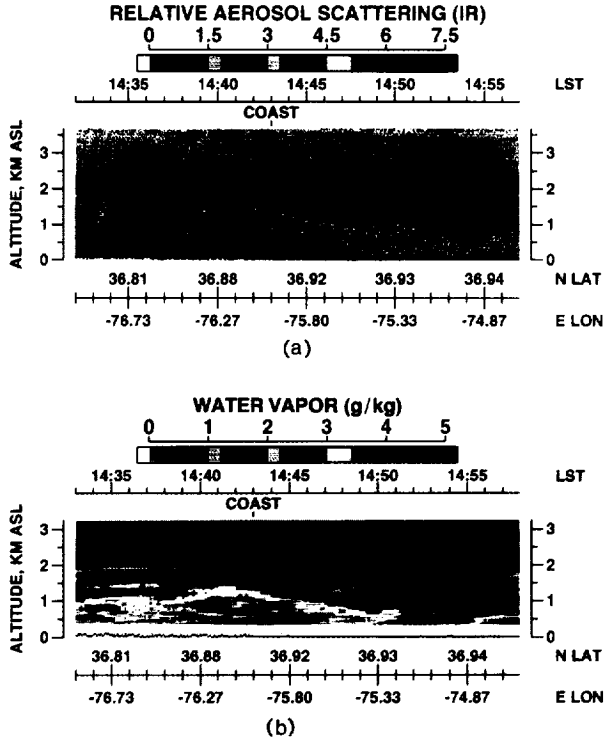

Fig. 10. Cross sections of (a) relative aerosol backscatter and (b) H_2O mass mixing ratio (grams per kilogram) obtained during a flight across the coast of Virginia on 22 March 1990. ASL, above sea level; LAT, latitude; LON, longitude.

near-simultaneous H_2O profiles from the DIAL system, the EG&G 300 dew-point hygrometer, and a radiosonde launched from the WFF ground station. Results from these measurements, which are presented in Fig. 11, verified the capability of the DIAL system to provide an accurate determination of the H_2O distribution from an aircraft altitude of almost 6

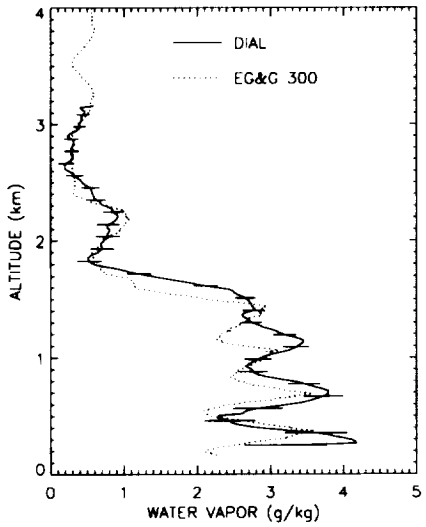

Fig. 9. Comparison of the DIAL and the DPT 300 hygrometer mixing ratio profiles over Emporia, Virginia, from an afternoon flight on 22 March 1990.

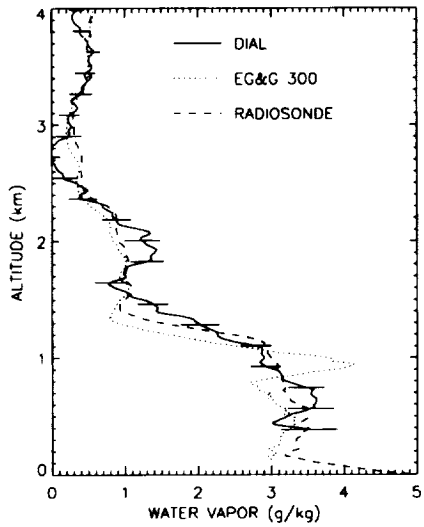

Fig. 11. Intercomparison of H_2O measurements with the DIAL system, the DPT 300 hygrometer, and a Vaisala radiosonde over the Wallops Flight Facility (WFF) at the end of the flight on 22 March 1990.

km. In addition, the comparison of the radiosonde and the hygrometer demonstrates good agreement between these two measurement techniques and allows us to be confident in using these instruments to verify the performance of the DIAL system.

A daytime flight was conducted across a cold front on 2 April 1990 to observe the difference in the H_2O structure on the wet side and on dry side of the front. In this case the weaker H_2O absorption line was used because of the high levels of H_2O on the warm side of the front. Measurements in the vicinity of the front were very difficult to achieve because of clouds and storm activity. However, farther from the front, clear conditions for DIAL measurements were available. One advantage of an airborne system is the flexibility of the aircraft in placing the instrument in locations that are favorable for DIAL measurements. Profiles obtained over Nashville, Tennessee, by use of the DIAL system, again with a 300-m range cell and the EG&G 300 hygrometer at 16:27 h LST, are shown in Fig. 12. The data shown in Fig. 12 are representative of the H_2O distribution on the dry side of the front because the front had passed over Nashville at approximately 14:00 h LST. It is clearly evident from this comparison that the DIAL system can make accurate measurements down to very low H_2O-concentration levels, even when using weaker absorption lines. It is expected that the accuracy of the low concentration level measurements would have been greater if the stronger H_2O line had been used. The H_2O cross-section data from this flight experiment indicated that the mixed layer height was limited to altitudes of 2 km and below on the dry side of the front. However, the H_2O mixing ratios approximately doubled on the warm side of the front, and the boundary-layer ceiling increased to approximately 3 km. These data show how the DIAL system can measure widely varying H_2O distributions that extend across different meteorological environments.

In addition to DIAL H_2O profiles, the system also measures the atmospheric scattering ratio by use of the off-line laser return signal, as described above. However, because the DIAL system usually operated in the nadir mode from an altitude of 4–5 km, it was very difficult to find an aerosol-free region for normalization. As a result, the actual scattering ratios are somewhat higher than those that were calculated, depending on how clean the atmosphere was at the normalization altitude. On the other hand, even relative measurements of the scattering ratio can provide very useful information. An example of a scattering-ratio profile is presented in Fig. 13, along with the corresponding H_2O plot from a flight on 16 April 1991. The scattering-ratio scale is delineated across the top of Fig. 13. The layer at 2 km, which could be a cloud, has a peak scattering ratio of 2. A scattering ratio of 2 signifies that 50% of the return signal is due to molecular (Rayleigh) scattering and 50% is backscattered by aerosols (Mie). Because this value could be underestimated, the signal from the aerosols is probably greater than that from the molecules. The plots shown in Fig. 13 indicate the general correlation of elevated H_2O levels with regions of higher aerosol loading.

The final set of data is shown to illustrate further the superior performance and operational capabilities of the H_2O DIAL system when an APD is used as the detector. Figure 14 presents two H_2O mixing ratio cross sections measured during a nighttime flight on 18 April 1991. The vertical range cell (210 m) and the horizontal averaging interval (2 min) are the same for both cross sections. Figure 14(a) shows measurements from an altitude of 4.5 km, with the PMT mounted in the receiver system. In this case the aircraft was flying north along the Eastern Shore of

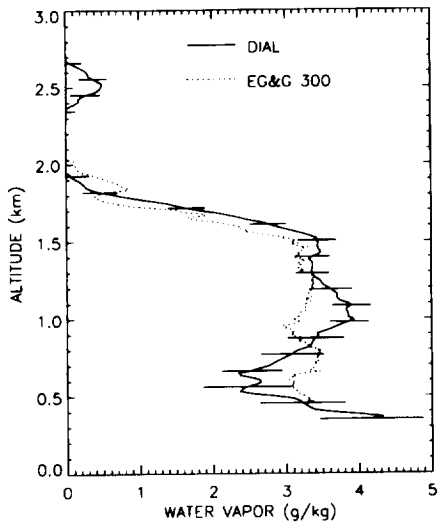

Fig. 12. Comparison of the DIAL and the DPT 300 hygrometer mixing ratios over Nashville, Tennessee, during a daytime flight on 2 April 1990. The profiles were obtained on the dry side of a cold front.

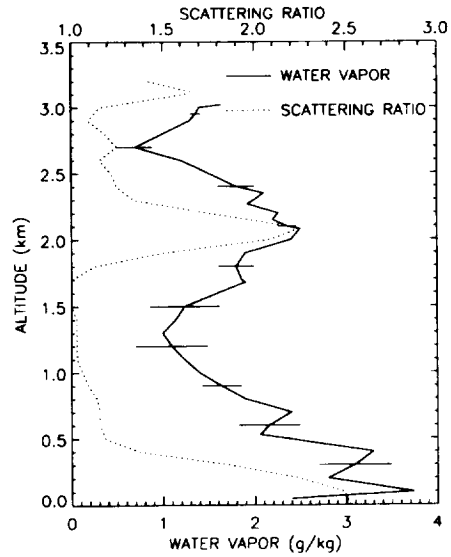

Fig. 13. Comparison of the H_2O mixing ratio and scattering ratio profiles from measurements performed during the daytime on 16 April 1991.

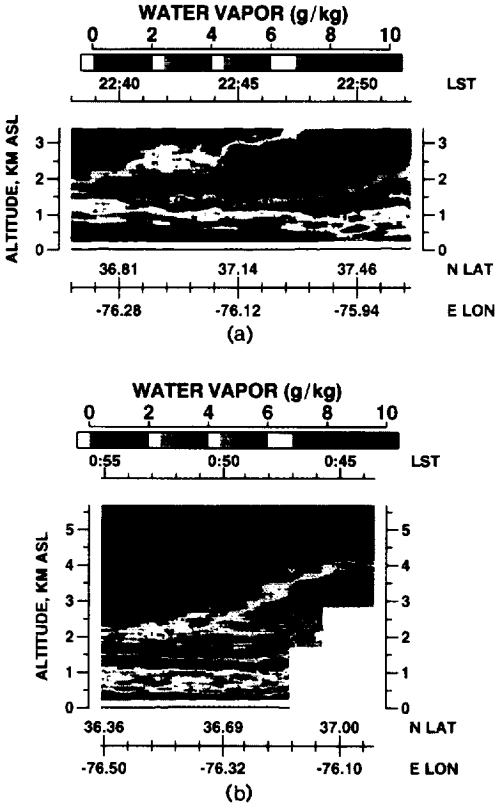

Fig. 14. Cross sections of H_2O mixing ratio distributions obtained during a flight along the Eastern Shore of Virginia on 18 April 1991 by use of (a) a PMT detector in the receiver system (flying north at an altitude of 4.5 km) and (b) an APD detector in the receiver system (flying south at an altitude of 7.1 km; the APD plot has been reversed for easier comparison with the PMT plot).

Virginia toward a storm system located over WFF (the storm edge is at approximately 37.7 °N latitude). Of particular interest is the signifcant increase in H_2O levels in the vicinity of the storm clouds, which has been observed by use of airborne *in situ* H_2O instruments.[38] For the plot shown in Fig. 14(b), the PMT had been replaced with an APD and the plane was flying south (the plot has been reversed for easier comparison with the PMT cross section) away from the storm system at an altitude of 7.1 km. The edge of the storm was then located at approximately 36.8 °N latitude, and the Electra was able to fly above the clouds near the edge of the storm. Again, as shown in Fig. 14(b), the increase in H_2O levels is readily apparent in the regions that surround the clouds. A 2-min interval ($\approx$ 12 km) of data from each of the two cross-section plots was used to generate a comparison of the performance of the system with the APD and the PMT. The approach used to compare the H_2O distribution measurements is similar to the approach used in the receiver detector section, and the results are shown in Fig. 15. Although the measurements are separated in time by approximately 1.5 h, the absolute amount of H_2O is relatively unchanged. Thus an accurate comparison of the performance of the system is possible by use of these

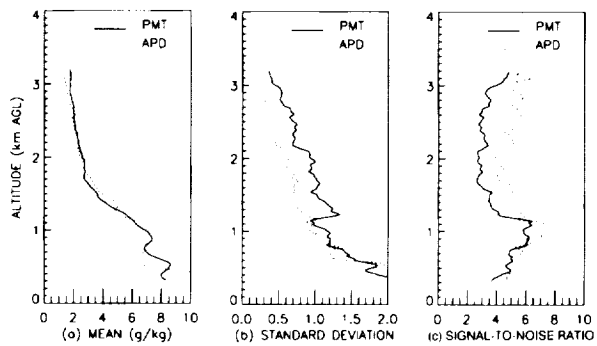

Fig. 15. Performance comparison of APD (aircraft altitude 7.1 km) and PMT (aircraft altitude 4.5 km) from a flight on 18 April 1991. The plots show (a) the measured mixing ratio profiles, (b) the mixing ratio standard deviation profiles (APD profile adjusted for range difference), and (c) the mixing ratio S/N profiles.

data. Because the aircraft altitude is higher for the APD measurements, the APD standard deviation profile was adjusted to compensate for the difference in the range from the aircraft to the measurement point. It is readily evident from Fig. 15 that the S/N for the APD is higher by 50–80% above 1000 m and is comparable with the PMT S/N below this altitude.

Summary and Conclusions

The NASA LaRC airborne H_2O DIAL system was designed and developed to perform investigations of a wide variety of atmospheric processes by providing accurate, high-resolution measurements of H_2O and aerosol distributions. This paper has described the H_2O DIAL system and its operation, presented data from the initial flight-test experiments, and evaluated the system performance. Included in these flights were to our knowledge the first airborne mesoscale H_2O DIAL measurements across a cold front, as well as the first measurements of this type in the vicinity of a large storm system. Numerous *in situ* H_2O profile measurements were performed during the flight tests for comparison with the H_2O profiles that were acquired by use of the DIAL system. These intercomparisons demonstrate the capability of the DIAL system to measure H_2O mixing ratios to better than $\pm 10\%$ in diverse atmospheric conditions. Currently the system is in a major development phase in which the Nd:YAG-pumped dye laser is being replaced with a second alexandrite laser as the off-line transmitter. In addition, both alexandrite lasers will be injection seeded with diode lasers, and the on-line transmitter will be stabilized on an adjustable H_2O line by use of an active wavelength-modulation technique. In the future the H_2O DIAL system will be used in major field experiments aimed at investigation of large-scale tropospheric and lower stratospheric processes, and this instrument will provide unique insight into the atmospheric variability of H_2O and aerosols.

The authors express their appreciation to the following people for their involvement in the development and the flight tests of the system: Byron Meadows

for his knowledgeable and dedicated technical assistance; Mark Jones, Bill McCabe, and Jerry Williams for their skilled technical support; John Barrick for his assistance in installing and operating the dewpoint hygrometers, as well as his helpful comments on interpreting their results; Marta Fenn, Susan Kooi, and Greg Nowicki for the DIAL data reduction and analysis; Roger Navarro, Dave Pierce, Doug Young, and the aircraft crew for their cooperation in conducting the flights; Riley Bull and his staff for providing the radiosonde data at WFF; and Carl Purgold and Bob Wheeler for assisting with the LaRC radiosondes. Special thanks to Joy Duke and Sandra Keyes for their patience in preparing this manuscript. This research was funded by NASA's Atmospheric Dynamics Program.

References

1. R. M. Schotland, "Some observations of the vertical profile of water vapor by means of a ground based optical radar," presented at the Fourth Symposium on Remote Sensing of the Environment, Ann Arbor, Mich., 12–14 April 1966.
2. S. H. Melfi, J. D. Lawrence, Jr., and M. P. McCormick, "Observation of Raman scattering by water vapor in the atmosphere," Appl. Phys. Lett. **15,** 295–297 (1969).
3. J. A. Cooney, "Remote measurements of atmospheric water vapor profiles using the Raman component of laser backscatter," J. Appl. Meteorol. **9,** 182–184 (1970).
4. E. V. Browell, J. D. Wilkerson, and T. J. McIlrath, "Water vapor differential absorption lidar development and evaluation," Appl. Opt. **18,** 3474–3483 (1979).
5. W. B. Grant, "Differential absorption and Raman lidar for water vapor profile measurements: a review," Opt. Eng. **30,** 40–48 (1991).
6. C. Cahen, J. L. Lesne, P. Deschamps, and P. Y. Thro, "Testing the mobile meteorological DIAL system for humidity and temperature monitoring," presented at the Fourteenth International Laser Radar Conference, San Candido, Italy, 24–26 June 1988.
7. S. H. Melfi, D. Whiteman, and R. Ferrare, "Observations of atmospheric fronts using Raman lidar moisture measurements," J. Appl. Meteorol. **28,** 789–806 (1989).
8. J. Boesenberg, "A DIAL system for high resolution water vapor measurements in the troposphere," in *Laser and Optical Remote Sensing: Instrumentation and Techniques,* vol. 18 of 1987 OSA Technical Digest Series (Optical Society of America, Washington, D.C., 1987), pp. 22–25.
9. N. S. Higdon, E. V. Browell, P. Ponsardin, T. H. Chyba, B. E. Grossmann, C. F. Butler, M. A. Fenn, S. D. Mayor, S. Ismail, and W. B. Grant, "Airborne water vapor DIAL research: system development and field measurements," presented at the Sixteenth International Laser Radar Conference, Boston, Mass., 20–25 July 1992.
10. G. Ehret, C. Kiemle, W. Renger, and G. Simmet, "Airborne remote sensing of tropospheric water vapor with a near-infrared differential absorption lidar system," Appl. Opt. **32,** 4534–4551 (1993).
11. R. T. H. Collis and P. B. Russell, "Lidar measurement of particles and gases by elastic backscattering and differential absorption," in *Laser Monitoring of the Atmosphere,* E. D. Hinkley, ed. (Springer-Verlag, New York, 1976), pp. 117–151.
12. R. M. Measures, *Laser Remote Sensing: Fundamentals and Applications* (Wiley, New York, 1984).
13. R. M. Schotland, "Errors in the lidar measurement of atmospheric gases by differential absorption," J. Appl. Meteorol. **13,** 71–77 (1974).
14. E. E. Remsberg and L. L. Gordley, "Analysis of differential absorption lidar from the Space Shuttle," Appl. Opt. **17,** 624–630 (1978).
15. C. Cahen and G. Megie, "A spectral limitation of the range resolved differential absorption lidar technique," J. Quant. Spectrosc. Radiat. Transfer **25,** 151–157 (1981).
16. S. Ismail and E. V. Browell, "Airborne and spaceborne lidar measurements of water vapor profiles: a sensitivity analysis," Appl. Opt. **28,** 3603–3615 (1989).
17. B. E. Grossmann and E. V. Browell, "Water vapor line broadening and shifting by air, nitrogen, oxygen, and argon in the 720-nm wavelength region," J. Mol. Spectrosc. **138,** 562–595 (1989).
18. B. E. Grossmann and E. V. Browell, "Spectroscopy of water vapor in the 720-nm wavelength region: line strengths, self-induced pressure broadenings and shifts, and temperature dependence of linewidths and shifts," J. Mol. Spectrosc. **136,** 264–294 (1989).
19. E. V. Browell, A. F. Carter, and T. D. Wilkerson, "An airborne differential absorption lidar system for water vapor investigations," Opt. Eng. **20,** 84–90 (1981).
20. E. V. Browell, "Remote sensing of tropospheric gases and aerosols with an airborne DIAL system," in *Optical Laser Remote Sensing,* D. K. Killinger and A. Mooradian, eds. (Springer-Verlag, New York, 1983), pp. 138–147.
21. P. Ponsardin, N. S. Higdon, B. E. Grossmann, and E. V. Browell, "Optimization of the alexandrite laser tuning elements for a water vapor lidar," in *Laser Radar V,* R. J. Becherer, ed., Proc. Soc. Photo-Opt. Instrum. Eng. **1222,** 178–182 (1990).
22. P. Ponsardin, N. S. Higdon, B. E. Grossmann, and E. V. Browell, "Stabilization and spectral characterization of an alexandrite laser for water vapor lidar measurements," in *Advanced Solid-State Lasers,* vol. 10 of OSA Proceedings (Optical Society of America, Washington, D.C., 1991), pp. 76–78.
23. P. Ponsardin, N. S. Higdon, B. E. Grossmann, and E. V. Browell, "Spectral control of an alexandrite laser for an airborne water vapor DIAL system," Appl. Opt. **33,** 6433–6444 (1994).
24. E. V. Browell, A. F. Carter, S. T. Shipley, R. J. Allen, C. F. Butler, M. N. Mayo, J. H. Siviter, Jr., and W. M. Hall, "NASA multipurpose airborne DIAL system and measurements of ozone and aerosol profiles," Appl. Opt. **22,** 522–534 (1983).
25. F. Bos, "Versatile high-power single-longitudinal-mode pulsed dye laser," Appl. Opt. **20,** 1886–1890 (1981).
26. "American National Standard for the Safe Use of Lasers," ANSI Z136.1-1986 (American National Standards Institute, New York, 1986).
27. S. Ismail and E. V. Browell, "Influence of rotational Raman scattering in DIAL measurements," presented at the Fourteenth International Laser Radar Conference, San Candido, Italy, 24–26 June 1988.
28. R. L. Kenimer, "Predictions of silicon avalanche photodiode performance in water vapor differential absorption lidar, in *Airborne and Spaceborne Lasers for Terrestrial Geophysical Sensing,* F. Allario, ed., Proc. Soc. Photo-Opt. Instrum. Eng. **889,** 126–135 (1988).
29. S. Ismail and E. V. Browell, "Recent technology developments and their influence on measurements of tropospheric water vapor," J. Atmos. Oceanic Technol. in press
30. S. Ismail, E. V. Browell, W. M. Hall, and R. L. Kenimer, "Signal processing and data smoothing influences in DIAL measurements," in *Optical Remote Sensing of the Atmosphere,* vol. 4 of OSA Proceedings (Optical Society of America, Washington, D.C., 1990), pp. 243–246.
31. C. F. Butler, "Theory and operation of the real-time data acquisition system for the NASA LaRC differential absorption

lidar (DIAL)," Tech. Rep. GSTR-88-1 (Old Dominion University, Norfolk, Va., 1988).
32. N. S. Higdon, E. V. Browell, P. Ponsardin, and B. E. Grossmann, "Airborne water vapor DIAL system development," in *Laser Radar V*, R. J. Becherer, ed., Proc. Soc. Photo-Opt. Instrum. Eng. **1222,** 183–185 (1990).
33. E. V. Browell, N. S. Higdon, C. F. Butler, M. A. Fenn, B. E. Grossmann, P. Ponsardin, W. B. Grant, and A. S. Bachmeier, "Tropospheric water vapor measurements with an airborne lidar system," presented at the Seventh American Meteorological Society Symposium on Meteorological Observations and Instrumentation, New Orleans, La, 14–18 January 1991.
34. F. Routhier and D. D. Davis, "Free tropospheric/boundary-layer airborne measurements of H_2O over the latitude range of 58 °S to 70 °N: comparison with simultaneous ozone and carbon monoxide measurements," J. Geophys. Res. **85,** 7293–7306 (1980).
35. S. H. Melfi, D. Whiteman, R. Ferrare, and F. Schmidlin, "Comparison of lidar and radiosonde measurements of atmospheric moisture profiles," in *Optical Remote Sensing of the Atmosphere*, vol. 4 of OSA Proceedings (Optical Society of America, Washington, D.C., 1990), pp. 232–234.
36. E. V. Browell, S. Ismail, and B. E. Grossmann, "Temperature sensitivity of differential absorption lidar measurements of water vapor in the 720-nm region," Appl. Opt. **30,** 1517–1524 (1991).
37. S. R. Drayson, "Rapid computation of the Voigt profile," J. Quant. Spectrosc. Radiat. Transfer **16,** 611–614 (1976).
38. L. F. Radke and P. V. Hobbs, "Humidity and particle fields around some small cumulus clouds," J. Atmos. Sci. **48,** 1190–1193 (1990).